Nazim Ucar*, Sule Dogan, Mustafa Serdar Karakas and Adnan Calik

Boriding of Binary Ni–Ti Shape Memory Alloys

DOI 10.1515/zna-2016-0289
Received August 2, 2016; accepted September 18, 2016; previously published online October 24, 2016

Abstract: Boriding of binary Ni–Ti shape memory alloys was carried out in a solid medium at 1273 K for 2, 4, 6, and 8 h using the powder pack method with proprietary Ekabor–Ni powders. Characterization of the boride layer formed on the surface of alloys was done by optical microscopy and scanning electron microscopy. The presence of boride, silicide, and borosilicide phases in the boride layers was confirmed by X-ray diffraction analysis. The thickness and microhardness of the boride layers increased with increasing boriding time. Hardness profiles showed a rapid decrease in hardness moving from the boride layer to the main structure. The high hardness of the boride layer was attributed mainly to the formation of TiB_2. A parabolic relationship was observed between layer thickness and boriding time, and the growth rate constant for the boriding treatment was calculated as 0.62×10^{-8} cm^2 s^{-1}.

Keywords: Boriding; Hardness Testing; Kinetics; Ni–Ti Shape Memory Alloys; X-Ray Diffraction.

1 Introduction

Important design considerations for engineering materials include properties such as high yield strength, hardness, corrosion, and wear resistance [1–4]. Widely used methods for improving these properties include surface modifications such as carburizing, boriding, and nitriding [5–7]. Boriding is a diffusional surface modification technique which involves the enrichment of the surface of a workpiece with boron by means of thermo-chemical treatment [1, 8, 9]. It is well known that the borided layer obtained has high hardness, good wear, and corrosion and oxidation resistance [10–12]. In many studies [13, 14] it has been indicated that the surface hardness of the resulting boride layer can exceed 2000 HV due to hard boride phases formed in the boride layer of steels. Previous studies have shown that the wear and corrosion behaviour of the steels can be improved by about 25 and 95 times, respectively, by the boriding treatment compared with untreated steel [15]. On the other hand, it has also been pointed out [16–18] that the thickness of a boride layer depends strongly on the boriding time, the boriding temperature, and the techniques used, such as gas, plasma, liquid, and pack boriding, as well as the chemical composition of the material to be borided.

Ni–Ti alloys with compositions near equiatomic concentration are well known for their shape memory characteristics. Effects of alloying additions such as copper and hafnium on the transformation characteristics in these alloys have been extensively studied and documented [19–22]. For example, it has been shown that the addition of Cu as a ternary alloying element results in an increase in the characteristic temperatures of the martensitic transformation, compared to binary Ni–Ti alloys [23]. In addition to their excellent shape memory characteristics, Ni–Ti alloys have been shown to display good combinations of other properties including strength, ductility, resistance to corrosion, and biocompatibility, which can be of considerable importance in a variety of engineering applications [24]. A number of studies have previously been carried out on microstructural characterization and mechanical properties of shape memory alloys, in both bulk [25, 26] and thin film forms [27–29]. However, there are currently very few studies regarding the boriding behaviour of binary Ni–Ti shape memory alloys. Therefore, the purpose of this work is to investigate the boriding behaviour of binary Ni–45.6 wt.% Ti shape memory alloys and to observe how the microstructure and mechanical properties of the alloy changes with boriding time. The results of the current study indicate that silicides and borosilicides can form alongside borides in the pack-boriding of Ni–Ti alloys of near-equiatomic concentration.

2 Experimental Method

Binary Ni–45.6 wt.% Ti shape memory alloys used in this study were initially cut in the dimensions of $2\times2\times10$ mm^3. The boriding treatments were carried out in a solid medium at 1273 K for 2, 4, 6, and 8 h using the powder pack method with Ekabor–Ni powders (BorTech

***Corresponding author: Nazim Ucar,** Physics Department, Faculty of Arts and Sciences, Suleyman Demirel University, Isparta, Turkey, E-mail: nazimucar@sdu.edu.tr
Sule Dogan: Physics Department, Faculty of Arts and Sciences, Suleyman Demirel University, Isparta, Turkey
Mustafa Serdar Karakas: Materials Science and Engineering Department, Faculty of Engineering, Cankaya University, Ankara, Turkey
Adnan Calik: Manufacturing Engineering Department, Faculty of Technology, Suleyman Demirel University, Isparta, Turkey

GmbH, Hürth, Germany). The samples were packed with the powders in hermetically sealed stainless steel containers and borided using an electrical resistance furnace. The boriding pack was ensured to have sufficient thickness (at least 25 mm) all around the sample. Metallographic sections were prepared to observe microstructural details by optical and scanning electron microscopy (SEM) (JEOL 5600LV). The thickness of borides was measured by means of a digital thickness measuring instrument attached to an optical microscope (Nikon MA100). The boride layer thickness values given in Section 3 are averages of at least 12 measurements. The presence of borides and other phases formed on the surface of the borided alloys was determined by using an X-ray diffractometer (Rigaku D-MAX 2200) with CuKα radiation of 0.15418 nm wavelength. To determine the hardness of the alloys, microhardness measurements were made on cross sections perpendicular to the borided surface by means of Vickers indenter with a load of 100 g and dwell time of 15 s. Before microhardness testing, a standard specimen was used for calibration. To ensure the reliability of the results, a minimum of five measurements were made at each depth to obtain an average hardness value.

3 Results and Discussion

SEM cross-sectional examinations of borided binary Ni–45.6 wt.% Ti shape memory alloys surfaces shown in Figure 1 revealed that the boride layer exhibits a smooth, compact morphology. The boride layer thickness versus time plot for the borided specimens is shown in Figure 2. The thickness of the boride layers for the borided binary Ni–45.6 wt.% Ti shape memory alloys ranged from 32 to 123 μm depending on boriding time.

The pack boriding of the binary Ni–45.6 wt.% Ti shape memory alloys using powder Ekabor–Ni powders led to the formation of a boride layer consisting mainly of titanium diboride (TiB_2). In many studies it has been

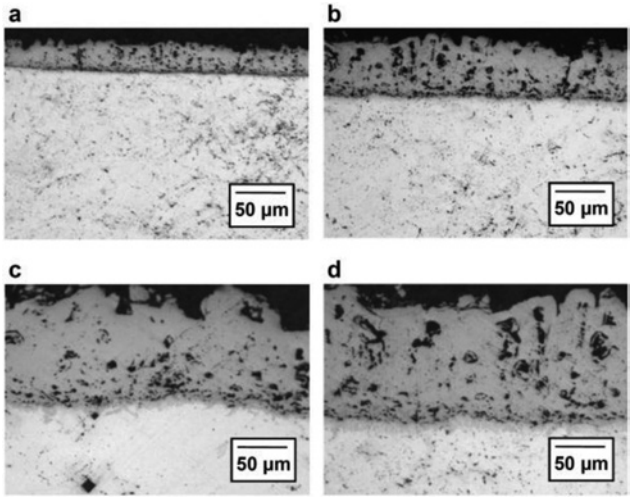

Figure 1: Cross-section views of binary Ni–45.6 wt.% Ti shape memory alloys borided for (a) 2, (b) 4, (c) 6, and (d) 8 h at 1273 K.

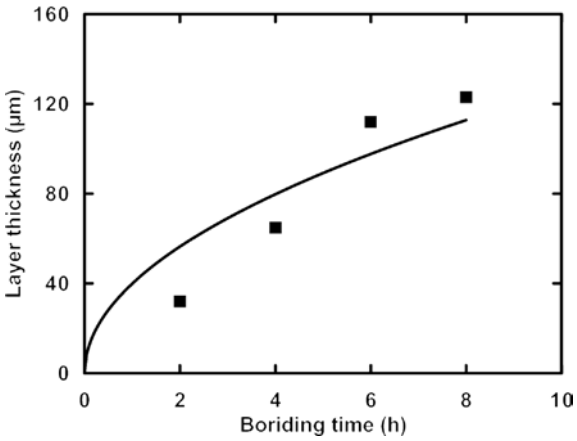

Figure 2: Boride layer thickness versus boriding time curve for the borided Ni–45.6 wt.% Ti shape memory alloys.

indicated that the conventional pack boriding process generally produces a dual layer consisting of TiB_2 and titanium monoboride (TiB) or a single layer of TiB depending on powder and/or alloy composition [30–32].

TiB_2 is considered an excellent choice for reinforcing titanium due to its high melting point, exceptional hardness, and high temperature oxidation resistance. It usually forms on the surface as a continuous monolithic layer with hardness of about 3400 HV. TiB on the other hand is known to form as long, pristine single-crystal whiskers underneath the TiB_2 layer penetrating into the titanium matrix with hardness of about 1600 HV [33–38].

Figure 1 shows the layer formed on the surface of the Ni–45.6 wt.% Ti shape memory alloys which was composed mainly of the TiB_2 phase. A very thin layer of whisker morphology was observed beneath the TiB_2 layer in the specimens borided for 6–8 h, indicative of possible TiB formation. Spalling was not observed in the boride

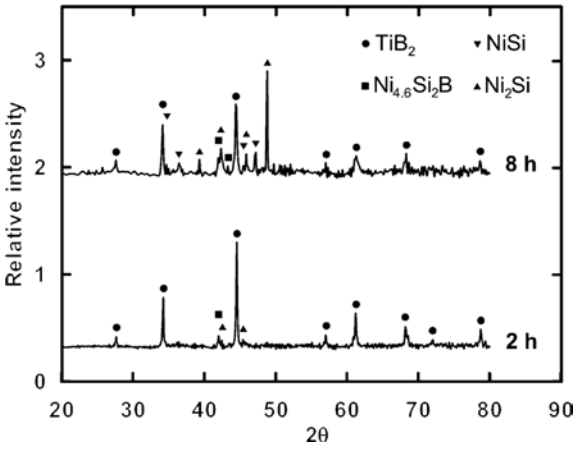

Figure 3: Diffraction patterns of binary Ni–45.6 wt.% Ti shape memory alloys borided for 2 and 8 h.

layer yet some porosity was present, probably as a result of differences in molar volume between the Ni–Ti alloy substrate and the TiB_2 phase.

X-ray diffraction (XRD) patterns for the Ni–Ti specimens borided for 2 and 8 h are shown in Figure 3. Both of the patterns clearly show the presence of TiB_2. However, the presence of TiB beneath the TiB_2 could not be verified. It is likely that either the peaks for the TiB phase were overwhelmed by the presence of other phases or the X-ray penetration depth was too shallow to detect the very thin sublayer. Other phases detected on the surface of the borided specimens mainly included silicides and borosilicides of nickel. These phases formed due to the additional presence of SiC in the boriding powders, which is used as a diluent for the boriding source (B_4C). These phases were identified as Ni_2Si, NiSi, and $Ni_{4.6}Si_2B$. The NiSi phase was not detected in the specimen borided for 2 h. It is well known that silicidization of nickel often results in the coexistence of nickel silicides Ni_2Si, NiSi, and Ni_5Si_2 [39–44] and that the presence of boron in addition to silicon can also result in the occurrence of borosilicides such as $Ni_{4.6}Si_2B$, $Ni_{4.29}Si_2B_{1.43}$, and Ni_6Si_2B [45–48].

Microhardness measurements were carried out from the surface to the interior on cross sections of the borided specimens. The microhardness profiles for all four Ni–45.6 wt.% Ti shape memory alloys borided from 2 to 8 h at 1273 K are shown in Figure 4. A very high value of 1995 $HV_{0.1}$ was measured in the cross section of the specimen borided for 8 h, confirming the presence of the compact TiB_2 layer. This value of hardness is similar yet somewhat lower than the values reported in other studies [33, 37], possibly due to porosity in the boride layer. The strong drop in hardness below the titanium boride layer corresponds to the results obtained by optical thickness measurements, indicating that boron diffuses further only to a small depth below the interface.

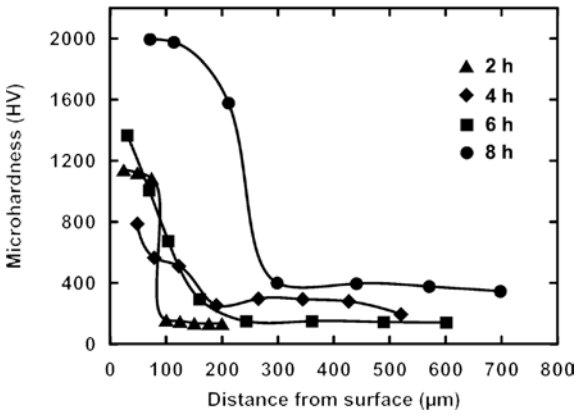

Figure 4: Hardness profiles for the borided Ni–45.6 wt.% Ti shape memory alloys.

Figure 4 also shows that the microhardness of the boride layer increases with increased boriding time due to the increased diffusion of boron. The hardness of the boride layer is much higher than that of the matrix for each boriding time. This is a consequence of the presence of hard TiB_2 phases as determined by XRD analysis. The obtained microhardness results are in agreement with those reported by several authors [8, 37–40].

The growth kinetics of the boride layers is controlled by the diffusion of boron into the substrate. The time dependence of boride layer thickness follows a parabolic growth law [41–43], given by the equation

$$d^2 = Kt \tag{1}$$

where d is the depth of the boride layer (μm), t is the boriding time (s), and K is the growth rate constant that depends on the diffusing species (in this case boron) and the diffusion coefficient. In the present study, the obtained effective growth rate constant with respect to boriding temperature 1273 K is 0.62×10^{-8} cm^2 s^{-1} for borided binary Ni–45.6 wt.% Ti shape memory alloys. Corresponding to this, the growth rate constants of pure Co [44], C15 carbon steel [45], and AISI H10 steel [46] have been obtained as 2.83×10^{-8} cm^2 s^{-1}, 2.0×10^{-8} cm^2 s^{-1}, and 0.11×10^{-8} cm^2 s^{-1}, respectively, for pack boriding carried out at 1273 K.

4 Conclusion

Boriding of binary Ni–45.6 wt.% Ti shape memory alloys was carried out with Ekabor–Ni powders for various durations at 1273 K. Based on the results, the following conclusions can be drawn:

- The boride layer exhibited a smooth, columnar morphology and consisted mainly of TiB_2. Traces of Ni_2Si, NiSi, and $Ni_{4.6}Si_2B$ were also detected from XRD patterns. TiB formation beneath the TiB_2 layer could not be verified.
- Nickel silicides formed simultaneously within the boride layer as a result of reaction between the alloy and the SiC diluent in the boriding source.
- A nearly parabolic relationship between layer thickness and boriding time was observed, and the depth of boride layer ranged from 32 to 123 μm. The growth rate constant for process was calculated as 0.62×10^{-8} cm^2 s^{-1}.
- The surface hardness values of the borided alloys were higher than those of untreated ones, and hardness

increased with increasing boriding time for both the boride layer and the transition layer.

Acknowledgments: This study was supported by the Scientific Research Projects Coordination Unit of Suleyman Demirel University (Project reference number: SDU-BAP 4290-YL1-15).

References

[1] A. Calik, A. Duzgun, A. E. Ekinci, S. Karakas, and N. Ucar, Acta Phys. Pol. A **116**, 1029 (2009).
[2] S. Danisman and S. Savas, Tribol. Ind. **27**, 41 (2005).
[3] M. Goune, T. Belmonte, A. Redjaimia, P. Weisbecker, J. M. Fiorani, et al., Mater. Sci. Eng. **A351**, 23 (2003).
[4] L. Shi and D. O. Northwood, Acta Mater. **43**, 453 (1995).
[5] C. H. Xu, J. K. Xi, and W. Gao, J. Mater. Process. Tech. **65**, 94 (1997).
[6] A. Calik, A. Duzgun, O. Sahin, and N. Ucar, Z. Naturforsch. **65a**, 468 (2010).
[7] P. X. Yan, Z. Q. Wei, X. L. Wen, Z. G. Wu, J. W. Xu, et al., Appl. Surf. Sci. **195**, 74 (2002).
[8] M. Kulka and A. Pertek, Appl. Surf. Sci. **214**, 161 (2003).
[9] R. Asthana, A. Kumar, and N. B. Dahotre, Materials Processing and Manufacturing Science, Butterworth-Heinemann, Oxford, UK, 2006, p. 313.
[10] I. Campos, O. Bautista, G. Ramírez, M. Islas, J. De La Parra, et al., Appl. Surf. Sci. **243**, 431 (2005).
[11] B. Venkataraman and G. Sundararajan, Surf. Coat. Tech. **73**, 177 (1995).
[12] H. J. Hunger and G. Trute, Heat Treat. Met. **21**, 31 (1994).
[13] I. Celikyurek, B. Baksan, O. Torun, and R. Gurler, Intermetallics **14**, 136 (2006).
[14] P. Jurci and M. Hudáková, J. Mater. Eng. Perform. **20**, 1180 (2011).
[15] E. Yilmaz, N. Ucar, A. Calik, S. Karakas, and R. Selbas, J. Balk. Trib. Assoc. **17**, 537 (2011).
[16] C. Li, B. Shen, G. Li, and C. Yang, Surf. Coat. Tech. **202**, 5882 (2008).
[17] C. Meric, S. Sahin, and S. S. Yilmaz, Mater. Res. Bull. **35**, 2165 (2000).
[18] I. Campos-Silva, M. Ortiz-Dominguez, C. Tapia-Quintero, G. Rodriguez-Castro, M. Y. Jimenez-Reyes, et al., J. Mater. Eng. Perform. **21**, 1714 (2012).
[19] A. J. Muir Wood, S. Sanjabi, Y. Q. Fu, Z. H. Barber, and T. W. Clyne, Surf. Coat. Tech. **202**, 3115 (2008).
[20] D. R. Angst, P. E. Thoma, and M. Y. Kao, J. Phys. IV **5**, 747 (1995).
[21] X. L. Meng, Y. F. Zheng, Z. Wang, and L. C. Zhao, Mater. Lett. **45**, 128 (2000).
[22] X. L. Meng, W. Cai, L. M. Wang, Y. F. Zheng, L. C. Zhao, et al., Scripta. Mater. **45**, 1177 (2001).
[23] T. Goryczka and J. Van Humbeeck, JAMME **17**, 65 (2006).
[24] M. T. Ochoa-Lara, H. Flores-Zúñiga, I. Estrada-Guel and R. Martínez-Sánchez, Microsc. Microanal. **11**, 1854 (2005).
[25] H. Pelletier, D. Muller, P. Mille, and J. J. Grob, Surf. Coat. Tech. **309**, 158 (2002).
[26] W. Ni, Y. T. Cheng, and D. S. Grummon, Appl. Phys. Lett. **80**, 3310 (2002).
[27] G. A. Shaw, D. S. Stone, A. D. Johnson, A. B. Ellis, and W. C. Crone, Appl. Phys. Lett. **83**, 257 (2003).
[28] W. Ni, Y. T. Cheng, M. Lukitsch, A. M. Weiner, L. C. Lev, et al., Wear **259**, 842 (2005).
[29] X. G. Ma and K. Komvopoulos, Appl. Phys. Lett. **83**, 3773 (2003).
[30] R. Filip, JAMME **15**, 174 (2006).
[31] B. Sarma, Accelerated Kinetics and Mechanism of Growth of Boride Layers on Titanium Under Isothermal and Cyclic Diffusion, PhD Thesis, Department of Metallurgical Engineering, University of Utah, UT, USA 2011, p. 30.
[32] K. S. Ravi Chandran, K. B. Panda, and S. S. Sahay, JOM-J. Min. Met. Mat. S. **56**, 42 (2004).
[33] C. Lee, A. Sanders, N. Tikekar, and K. S. Ravi Chandran, Wear **265**, 375 (2008).
[34] N. M. Tikekar, K. S. Ravi Chandran, and A. Sanders, Scripta. Mater. **57**, 273 (2007).
[35] P. Chandrasekar, V. Balusamy, K. S. Ravi Chandran, and H. Kumar, Scripta. Mater. **56**, 641 (2007).
[36] S. Aich and K. S. Ravi Chandran, Metall. Mater. Trans. A **33**, 3489 (2002).
[37] P. Kaestner, J. Olfe, and K.-T. Rie, Surf. Coat. Tech. **142–144**, 248 (2001).
[38] B. Sarma and K. S. Ravi Chandran, Acta Mater. **59**, 4216 (2011).
[39] K. Maex and M. van Rossum, Properties of Metal Silicides, INSPEC, the Institution of Electrical Engineers, London 1995, p. 113.
[40] D.-W. Deng, C.-G. Wang, Q.-Q. Liu, and T.-T. Niu, T. Nonferr. Metal Soc. **25**, 437 (2015).
[41] M. Kulka, N. Makuch, and M. Popławski, Surf. Coat. Tech. **244**, 78 (2014).
[42] D. Mu, B.-L. Shen, C. Yang, and X. Zhao, Vacuum, **83**, 1481 (2009).
[43] I. Ozbek, H. Akbulut, S. Zeytin, C. Bindal, and H. Ucisik, Surf. Coat. Tech. **126**, 166 (2000).
[44] S.-Y. Tan, C.-Y. Hu, H.-C. Chiu, C.-W. Feng, I.-T. Chen, et al., IEEE Conference on EDSSC, Taiwan, 2007, p. 165.
[45] J. Grabis, D. Rašmane, A. Krūmiņa, and A. Patmalnieks, Mater. Sci. Medzg. **18**, 72 (2012).
[46] E. Lugscheider and H. Reimann, Monatsh. Chem. **106**, 1155 (1975).
[47] T. Tokunaga, K. Nishio, H. Ohtani, and M. Hasebe, Mater. Trans. **44**, 1651 (2003).
[48] N. Lebrun, P. Perrot, A. Serbruyns, J.-C. Tedenac, in: Refractory Metal Systems: Phase Diagrams, Crystallographic and Thermodynamic Data (Eds. G. Effenberg, S. Ilyenko), Springer, Berlin 2010, p. 133.